Anonymous Author(s)

Affiliation Address email

Abstract

3

4

5

6

8

9

11

12

13

14

15

16

17

18

19

Masked diffusion large language models (dLLMs) are emerging as promising alternatives to autoregressive LLMs, offering competitive performance while supporting unique generation capabilities such as *inpainting*. We explore how *inpainting* can inform RL algorithm design for dLLMs. Aligning LLMs with reinforcement learning faces an exploration challenge: sparse reward signals and sample waste when LLMs fail to discover correct solutions. While this inefficiency affects LLMs broadly, dLLMs offer a distinctive opportunity—their inpainting ability can guide exploration. We introduce IGPO (Inpainting Guided Policy Optimization), an RL framework that strategically injects partial ground-truth reasoning traces during online sampling. Unlike providing full solutions, inpainting steers exploration toward promising trajectory spaces while preserving self-generated reasoning, bridging supervised fine-tuning and reinforcement learning. We apply IGPO to group-based optimization methods such as GRPO, where exploration failures cause zero advantages and gradients. IGPO restores meaningful gradients while improving sample efficiency. We also propose supervised fine-tuning on synthetically rewritten concise traces that better align with dLLM generation patterns. With additional techniques including entropy-based filtering, our training recipe yields substantial gains across four mathematical benchmarks—GSM8K, Math500, AMC and Minerva—achieving new state-of-the-art results for full-attention masked dLLMs.

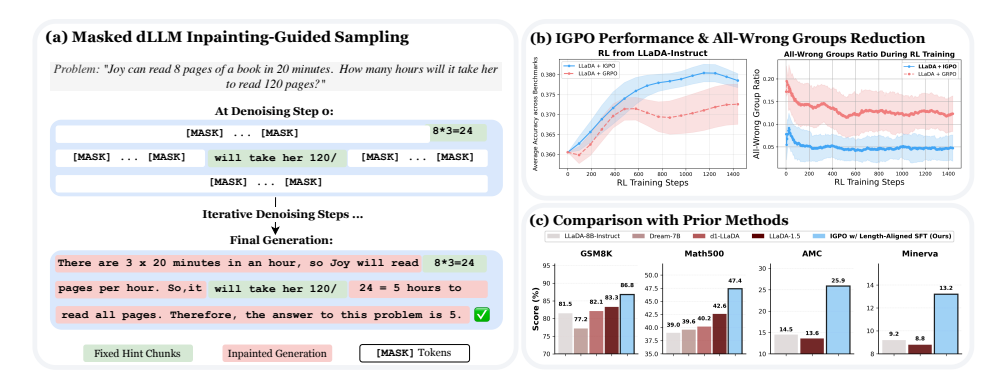


Figure 1: (a) Unlike autoregressive LLMs, diffusion LLMs can be conditioned on future reasoning hints during generation through *inpainting* via bidirectional attention, enabling guided exploration toward correct solutions. (b) Applying inpainting-guided exploration in policy optimization outperforms standard Group Relative Policy Optimization (GRPO) sampling and reduces all-wrong groups occurrences. (c) Our full training recipe combining *Length-Aligned* supervised fine-tuning on concise reasoning traces with IGPO achieves SoTA performance among full-attention masked dLLMs across four mathematical reasoning benchmarks.

1 Introduction

30

31

32

34

35

36

Recent research has shown that masked diffusion large language models (dLLMs) (Austin et al., 21 2021; Lou et al., 2024; Shi et al., 2024) such as LLaDA (Nie et al., 2025) and Dream (Ye et al., 2025) 22 can achieve performance competitive with autoregressive LLMs of similar size. Their capabilities and 23 performance can be further enhanced via RL post-training (Zhao et al., 2025; Gong et al., 2025b) and ability to flexibly include multimodal data (Li et al., 2025; Yang et al., 2025; You et al., 2025). Unlike 25 autoregressive LLMs, which decode in a left-to-right manner, dLLMs iteratively unmask tokens in 26 27 parallel. This brings potential for faster inference as shown in closed models like Mercury (Inception Labs et al., 2025) and Gemini Diffusion (DeepMind, 2025), along with a flexible inductive bias for 28 operations such as *inpainting*, the ability to fill in missing content within existing text. 29

In this work, we explore how *inpainting* can be leveraged to inform post-training algorithms for dLLMs. Recent work on post-training of dLLMs has adopted training approaches similar to autoregressive LLMs, applying Reinforcement Learning with Verifiable Reward (RLVR) methods (Zhao et al., 2025; Yang et al., 2025; Gong et al., 2025b). However, a fundamental exploration challenge persists: for challenging tasks, policies struggle to discover correct solutions and binary rewards provide minimal learning signal when most generated solutions are incorrect. This leads to substantial sample waste and poor training efficiency, exacerbating the computational costs of online RL.

The bidirectional generative structure of diffusion LLMs provides a unique mechanism to address this 37 exploration challenge. Since dLLMs are trained through stochastic masking patterns, they possess inherent capability for accepting externally provided partial hints through inpainting. We leverage 39 this ability to introduce IGPO (Inpainting Guided Policy Optimization), a novel RL framework that 40 strategically guides exploration for dLLMs by injecting reasoning hints when answering difficult 41 problems. Specifically, when the policy is unlikely to generate correct solutions, partial reasoning 42 traces are injected into the generation region, and the dLLM is tasked with completing the remaining 43 reasoning sequence and output final answer. The final answers are verified against ground truth, and 44 only successful completions are used for downstream policy optimization. 45

We demonstrate IGPO's effectiveness in group-based policy optimization methods such as 47 GRPO (Shao et al., 2024), which are particularly vulnerable to exploration failures: when a group's responses are all incorrect, group-normalized advantage collapses to zero and resulting in zero gradi-48 ents. This occurs with alarming frequency in challenging domains. By reducing the prevalence of 49 all-wrong groups, IGPO restores gradient signals and enables more effective RL. More broadly, IGPO 50 can be viewed as a form of *guided exploration* that interpolates between supervised and RL paradigms. 51 The injected tokens act as conditioning context that steers the policy's action distribution toward 52 high-reward regions. Unlike pure SFT, which might suffer from distribution shift between data and policy rollouts (Zhang et al., 2025), IGPO maintains on-policy generation for the non-injected tokens. Finally, we augment IGPO with techniques that improve learning stability and performance, including 55 entropy-based gradient filtering for injected tokens, and conduct comprehensive experiments across 56 math benchmarks. We evaluate each component of our approach through ablation studies. Our work 57 makes the following key novel contributions: 58

- We propose IGPO, the first work to utilize the unique inpainting capabilities of diffusion LLMs
 for reinforcement learning. By strategically injecting partial reasoning traces during exploration,
 IGPO alleviates the inefficiency of sparse verifiable rewards and mitigates the zero-advantage
 dilemma in group-based policy optimization methods, substantially reducing the proportion of
 all-wrong groups (by approximately 60% as shown in Fig 1 (b)) in our training.
- We propose a *Length-Aligned* SFT for full-attention based dLLMs using synthetically rewritten,
 concise reasoning traces. This design better aligns SFT data length with RL sampling and evaluation
 length, avoids the limitations of verbose traces, and provides stronger initialization for RL.
- Our full training recipe achieves substantial improvements on mathematical benchmarks, including +5.3% on GSM8K, +8.4% on Math500, +11.4% on AMC, and +4.0% on Minerva relative to the LLaDA-Instruct, achieving SoTA performance among full-attention based dLLMs.
- We conduct a comprehensive ablation study that disentangles the mechanisms of IGPO. We show that partial inpainting consistently outperforms full ground-truth inpainting by staying closer to the policy distribution in online RL, and propose an entropy-based gradient filtering mechanism that stabilizes training dynamics.

4 2 Preliminaries

2.1 Masked Diffusion Large Language Models

Masked diffusion LLMs (Austin et al., 2021; Sahoo et al., 2024; Shi et al., 2024; Ou et al., 2024; Lou 76 et al., 2024) employ a forward diffusion (masking) process that progressively corrupts clean sequences 77 x_0 by introducing mask tokens. This process is indexed by continuous time $t \in [0,1]$. At any timestep 78 $t \in (0,1)$, the partially corrupted sequence x_t is obtained by independently masking tokens so that each token remains unmasked with probability α_t , where the schedule α_t is strictly decreasing in t. At t=1, the sequence is fully masked. Training specifies the forward process via α_t and learns 81 a bidirectional unmasking predictor f_{θ} to recover the original tokens from x_t . Each step samples 82 $t \in [0,1)$, applies the forward masking to obtain $x_t \sim q_{t|0}(x_t|x_0)$, and optimizes a masked-token 83 objective derived from the negative evidence lower bound (NELBO), which upper-bounds the data negative log-likelihood (NLL). For masked dLLMs this NELBO reduces to a weighted NLL with 85 weights determined by transforms of α_t (Sahoo et al., 2024, Eq. (10)). For example, LLaDA (Nie et al., 2025) uses a linear schedule $\alpha_t = 1 - t$, leading to:

$$-\mathbb{E}_{t \sim \mathcal{U}[0,1), \ x_0 \sim p_{\text{data}}, \ x_t \sim q_{t|0}(x_t|x_0)} \left[\frac{1}{t} \sum_{k=1}^{|x_t|} \mathbb{1}[x_t^k = \text{mask}] \log f_{\theta}(x_0^k \mid x_t) \right], \tag{1}$$

where $|x_t|$ is the sequence length and x^k the k-th token. The loss is computed only on tokens masked at time t. For prompt-conditional generation, prompt tokens are kept unmasked while continuation tokens are initialized as mask. The model then simulates a reverse process $p_{\theta}(x_s \mid x_t)$ over timesteps t > s, where f_{θ} provides denoising predictions for masked positions. Throughout the reverse trajectory, already unmasked tokens are preserved and carried forward unchanged.

2.2 Policy Optimization for Masked Diffusion Large Language Models

Policy-gradient post-training is widely used for LLM alignment (Ouyang et al., 2022; Bai et al., 2022; Li et al., 2023; Ahmadian et al., 2024). GRPO (Shao et al., 2024; Guo et al., 2025; Team et al., 2025) is a value-free variant of PPO (Schulman et al., 2017) that uses group-wise, sequence-level advantages for G responses $\{o_i\}_{i=1}^G$ to a query q:

$$A_i = r(o_i) - \frac{1}{G} \sum_{j=1}^{G} r(o_j).$$
 (2)

The GRPO objective integrates ratio clipping and reverse-KL regularization:

$$\mathcal{L}_{GRPO}(\theta) = \mathbb{E}_{\substack{q \sim \mathcal{D} \\ o_1, \dots, o_G \sim \pi_{\theta_{old}}(\cdot|q)}} \left[\frac{1}{G} \sum_{i=1}^{G} \frac{1}{|o_i|} \sum_{k=1}^{|o_i|} \min\left(\rho_i^k A_i, \operatorname{clip}\left(\rho_i^k, 1 - \varepsilon, 1 + \varepsilon\right) A_i\right) - \beta D_{KL} \left[\pi_{\theta}(\cdot|q) \| \pi_{\text{ref}}(\cdot|q)\right] \right], \quad (3)$$

where $\rho_i^k = \frac{\pi_\theta(o_i^k|q,o_i^{< k})}{\pi_{\theta_{\rm old}}(o_i^k|q,o_i^{< k})}$ is the probability ratio, $r(\cdot)$ is a reward function, $\beta>0$ is the KL regularization coefficient, $\varepsilon>0$ is the clipping parameter, and $\pi_{\rm ref}$ is the reference policy. In autoregressive models, the reverse-KL is tractable via the chain rule, $\log \pi_{\rm AR}(o\mid q) = \sum_{k=1}^{|o|} \log \pi_{\rm AR}(o^k\mid q,o^{< k})$, but masked diffusion LLMs do not admit a left-to-right factorization because π_θ arises from composing reverse denoising steps of the mask predictor. To make GRPO practical for masked diffusion policies, DiffuGRPO (Zhao et al., 2025) adopts a mean-field approximation that yields single-pass estimators for token-level ratios and the reverse-KL; we use these estimators throughout. We provide a detailed background discussion in Section B.

3 Methods

107

108

93

3.1 IGPO: Inpainting Guided Policy Optimization

Zero-Advantage Dilemma. In the GRPO framework, when sampling G responses $\{o_1, o_2, \ldots, o_G\}$ for a given prompt q, the advantage computation relies on reward variance across the group. However, when all responses receive identical rewards—either all correct or all incorrect

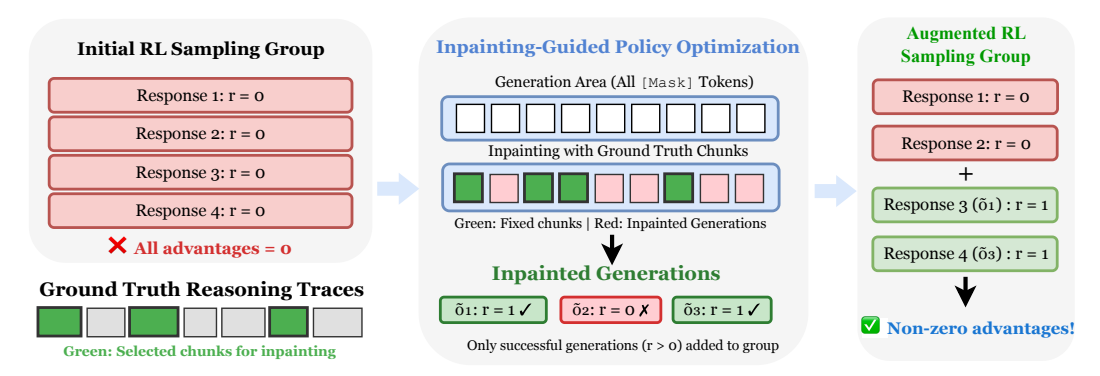


Figure 2: **Overview of IGPO:** When all sampled responses yield identical incorrect rewards (zero-advantage scenario), we perform hint-guided inpainting by generating additional responses using ground truth reasoning chunks as injected hints. Ground truth traces y^* are segmented into variable-length chunks, and selected chunks are injected as fixed hints during generation while the model generates the remaining tokens. We then replace a fraction of the original incorrect responses with correct responses generated through inpainting, creating reward variance that enables non-zero advantages for effective policy gradient updates.

the advantages become zero: $A_i = r(o_i) - \frac{1}{G} \sum_{j=1}^G r(o_j) = 0$. This zero-advantage scenario makes the policy gradient component degenerate. Specifically, the clipped surrogate objective collapses to zero regardless of whether the update lies in the clipped or unclipped region, since both terms contain $A_i = 0$. The policy gradient for this prompt q therefore becomes:

$$\frac{1}{G} \sum_{i=1}^{G} \frac{1}{|o_i|} \sum_{k=1}^{|o_i|} A_i \, \rho_i^k \, \nabla_\theta \log \pi_\theta(o_i^k \mid q) \ = \ 0 \qquad \text{since } A_i = 0 \, \forall i.$$

As a result, no meaningful policy update can be extracted from the reward signal, wasting compute sampling these responses. In this work, we specifically focus on mitigating the *all-wrong* case.

Masked dLLM Generation and Inpainting. In full-attention masked dLLM generation, the model input at denoising step 0 is the concatenation $[q; z_{\text{mask}}]$, where q represents the prompt and $z_{\text{mask}} = [\text{mask}, \text{mask}, \dots, \text{mask}]$ denotes a fully masked completion sequence of predetermined length L. The generation process progressively unmasks these positions through iterative denoising until producing the final output.

Hint injection modifies this formulation by fixing selected positions of z_{mask} to ground-truth tokens. During RL training, we assume access to ground-truth reasoning trace $y^* = [y_1^*, y_2^*, \dots, y_{|y^*|}^*]$ for

every question q. For injection, we create a binary mask $m \in \{0,1\}^L$ indicating which positions to inject as fixed hints, we construct the hint-injected initialization:

125

126

$$z^{\text{hint}}[i] = \begin{cases} y_i^* & \text{if } m[i] = 1 \text{ and } i \le |y^*|, \\ \text{mask} & \text{otherwise.} \end{cases}$$
 (4)

The masked dLLM then performs bidirectional denoising on $[q; z^{\text{hint}}]$ through the inpainting process, leveraging both the prompt and injected hint tokens to generate coherent responses. The injected hint tokens remain fixed throughout the iterative denoising steps.

Constructing Hint Patterns for Inpainting. To construct meaningful hint patterns for the inpainting process, we segment the ground truth reasoning trace y^* into variable-length contiguous chunks $\mathcal{C} = \{c_1, c_2, \ldots, c_N\}$, where each chunk length $|c_j|$ is sampled from $\mathcal{U}[s_{\min}, s_{\max}]$. We explicitly exclude the final answer tokens from chunking to prevent reward hacking behaviors where the model ignores reasoning and collapses. For a given hint injection ratio $\eta \in [0, 1]$, we randomly select $\lfloor \eta \cdot N \rfloor$ chunks and set their corresponding positions in the binary mask m to 1 for hint injection.

Algorithm 1 IGPO: Inpainting-Guided Policy Optimization for Masked dLLMs

```
Require: Reference model \pi_{ref}, prompt distribution \mathcal{D}, ground-truth reasoning traces \{y^*\}, number
     of completions per prompt G, number of inner updates \mu, hint injection ratio range [\eta_{\text{low}}, \eta_{\text{high}}],
     replacement fraction \lambda, entropy filter threshold \tau, chunk size range [s_{\min}, s_{\max}]
 1: Initialize \pi_{\theta} \leftarrow \pi_{\text{ref}}
 2: while not converged do
 3:
          \pi_{\text{old}} \leftarrow \pi_{\theta}; sample prompt q \sim \mathcal{D} and responses o_{1:G} \sim \pi_{\text{old}}(\cdot \mid q); compute rewards r_{1:G}
 4:
          if all r_i = 0 (zero-advantage case) then
               Segment ground-truth reasoning y^* into chunks \{c_1, \ldots, c_N\} with |c_i| \sim \mathcal{U}[s_{\min}, s_{\max}]
 5:
 6:
                    Sample hint injection ratio \eta \sim \mathcal{U}[\eta_{\mathrm{low}}, \eta_{\mathrm{high}}] and select \lfloor \eta N \rfloor chunks from
     \{c_1,\ldots,c_N\} randomly
                    Inject selected chunk tokens as fixed hints at corresponding positions
 8:
 9:
                    Generate \tilde{o}_i via inpainting: denoise only masked positions, keep hint tokens fixed
10:
               Evaluate rewards r(\tilde{o}_i) and replace up to |\lambda G| incorrect o_i with correct \tilde{o}_i
11:
          Compute advantages A_i on the updated response set
12:
          for n=1,\ldots,\mu do
               Estimate \log \pi_{\theta}, \log \pi_{\text{old}}, \log \pi_{\text{ref}}; apply top-\tau entropy filter on hint positions
13:
14:
               Update \pi_{\theta} via \mathcal{L}_{IGPO}(\theta) (Eq. 5)
15: return \pi_{\theta}
```

Elastic Inpainting-Triggered Sampling. With the above inpainting setup, we design IGPO (as in Algorithm 1) to be elastic: hint injection is only triggered when all sampled responses in a group yield incorrect rewards (the zero-advantage case), and when activated, both the hint injection ratio η and chunk sizes ($\mathcal{U}[s_{\min}, s_{\max}]$) are randomized to provide diverse training signals. Concretely, when detecting that all sampled responses $\{o_1, \ldots, o_G\}$ for query q yield identical rewards $r(o_i) = 0$, we generate an additional set of responses $\{\tilde{o}_1, \ldots, \tilde{o}_G\}$ through the inpainting process. Each response \tilde{o}_i is generated via inpainting with a distinct hint injection ratio $\eta_i \sim \mathcal{U}[\eta_{\text{low}}, \eta_{\text{high}}]$ to ensure diverse hint densities. Following inpainting generation, we evaluate the correctness of $\{\tilde{o}_i\}$ and only use the correct ones for replacement. Specifically, we replace $K = \min(|\{\tilde{o}_i: r(\tilde{o}_i) = 1\}|, |\lambda G|)$ of the original incorrect responses with correct responses generated through inpainting, where $\lambda \in (0,1)$ controls the replacement fraction.

136

138

139

140

141

142

143

146

150

151

152

153

154

155

156

157

158

159

160

161

162

163

164

The complete IGPO objective modifies the GRPO formulation by incorporating the augmented sampling procedure:

$$\mathcal{L}_{\text{IGPO}}(\theta) = \mathbb{E}_{\substack{\{o_1, \dots, o_{G-K}, \check{o}_1, \dots, \check{o}_K\} \sim \text{IGPO-Sample}(\pi_{\theta}, q, y^*)}} \left[\left(\frac{1}{G} \sum_{i=1}^G \frac{1}{L_i} \sum_{k=1}^{L_i} \min \left(\rho_i^k A_i^k, \operatorname{clip} \left(\rho_i^k, 1 - \varepsilon, 1 + \varepsilon \right) A_i^k \right) \right) - \beta D_{\text{KL}} \left[\pi_{\theta}(\cdot | q) \| \pi_{\text{ref}}(\cdot | q) \right] \right], \tag{5}$$

where IGPO-Sample (π_{θ},q,y^*) denotes the augmented sampling procedure that applies inpainting-based augmentation when zero-advantage scenarios are detected, producing the augmented RL sampling group $\{o_1,\ldots,o_{G-K},\tilde{o}_1,\ldots,\tilde{o}_K\}$ containing (G-K) original responses and K verified correct inpainted responses $\{\tilde{o}_i\}$ after replacement. L_i denotes the length of the i-th response (whether o_i or \tilde{o}_i). Crucially, only inpainted responses that pass correctness verification are included in the augmented group, satisfying $r(\tilde{o}_i)=1$. Advantages A_i are computed normally. We built IGPO with DiffuGRPO (Zhao et al., 2025)'s log probability estimation methods, where all completion tokens are masked during estimation and we remove the random masking applied to prompt tokens as done in DiffuGRPO. Since we use a small number of policy iterations (i.e. $\mu=4$), this alleviates the need for random prompt masking to reduce overfitting. Inspired by Zheng et al. (2025), we compute sequence-level importance-ratio through mean-field approximation for stability purposes.

Entropy-based Gradient Filtering for Hint Tokens. When applying IGPO to zero-advantage scenarios, the responses generated through inpainting contain ground truth reasoning chunks that originate from a different distribution than the current policy π_{θ} . This creates an off-policy learning scenario where gradient updates from ground truth tokens can conflict with the model's current beliefs, particularly at positions where the model has high confidence (low entropy). To mitigate potential training instability from this distribution mismatch, we implement an entropy-based filtering approach that restricts learning to hint token positions where the model exhibits sufficient uncertainty,

as inspired by Huang et al. (2025). Specifically, for each hint token position (i.e., positions with 167 injected ground-truth tokens) we compute the entropy. We then apply gradient updates only to 168 the top τ percentile of hint token positions with highest entropy values. This selective learning 169 strategy serves two purposes: high-entropy positions represent genuine decision boundaries where 170 the model is naturally uncertain and thus more receptive to external guidance, and they correspond to 171 flatter probability distributions that yield more stable gradient updates when incorporating ground 172 173 truth information. This approach controls the policy shift by focusing learning on positions where the model is already open to change, rather than forcing updates against strong existing beliefs at 174 low-entropy positions. 175

3.2 Length-Aligned SFT via Concise Reasoning Trace Rewriting

To further strengthen our training recipe, we seek better RL initialization via SFT but identified 177 generation length mismatches across SFT, RL sampling, and evaluation phases. Full-attention masked dLLMs like LLaDA lack KV cache optimization (Wu et al., 2025) by defualt, requiring full-sequence attention at every denoising step, which dominates online RL training cost. As a result, we restrict RL 180 rollouts to 256 tokens for faster convergence within a reduced exploration space, and evaluation setups 181 in recent work (Zhao et al., 2025; Zhu et al., 2025; Nie et al., 2025) typically use 256-1024 tokens. In 182 contrast, popular reasoning SFT corpora (e.g., OpenR1) contain verbose traces often exceeding 10k 183 tokens, creating distribution mismatch across SFT, RL, and evaluation, and include repeated reflective 184 behaviors unsuited for limited context. To resolve this, we systematically rewrite verbose traces into 185 concise, structured forms that preserve logical flow while respecting dLLM computational limits. 186 Using LLaMA-4-Maverick (Meta, 2025) with prompts detailed in Section I, we remove redundant 187 reflections, condense multi-sentence elaborations into precise, mathematically rigorous statements, 188 and retain essential reasoning. Examples of revision length distributions and before/after traces are 189 in Sections D and I. Our Length-Aligned SFT trains LLaDA solely on rewritten traces, improving 190 RL initialization by avoiding implicit length compression and focusing learning on reasoning quality 191 within fixed compute budgets. Empirical results show clear gains over training on verbose traces, and 192 we further observe that masked dLLMs benefit from extended training (e.g., 100 epochs) relative to 193 AR LLMs, consistent with recent works (Ni and the team, 2025; Prabhudesai et al., 2025).

195 4 Experiments

176

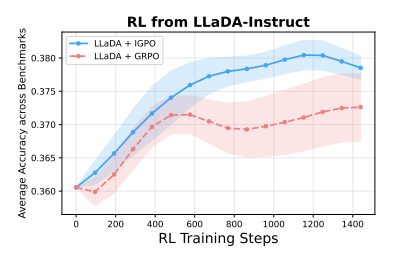
206

To investigate how the inpainting capabilities of masked dLLMs can address the exploration challenges in RL and how *Length-Aligned* SFT improves performance, we conduct comprehensive experiments to answer the following main research questions:

- 199 (1) How effectively does our complete training approach (Length-aligned SFT with rewritten reason-200 ing traces followed by reinforcement learning with IGPO) improve the mathematical reasoning 201 performance of LLaDA and reduce all-wrong groups occurrences? (§4.3)
- How does partial hint injection in IGPO bridge on-policy generation with ground truth guidance, and how does this improve learning compared to full supervision? (§4.4)
- How do key design choices—including entropy filtering thresholds and reasoning trace rewriting—affect RL training dynamics and learning stability? (§4.4)

4.1 Complete Training Recipe

Our complete learning framework consists of a two-stage pipeline: Stage 1: Supervised Fine-Tuning 207 with Rewritten Traces. We begin with Length-Aligned SFT on the LLaDA-8B-Instruct model using 208 the OpenR1-Math-220K dataset's default split (94k math problems), but with all reasoning traces 209 rewritten (See Section D for length distribution before and after revision). This ensures consistency 210 between training distribution and downstream RL/evaluation phases by aligning trace lengths. Stage 211 2: Reinforcement Learning with IGPO. Following Length-aligned SFT, we apply IGPO to further 212 enhance reasoning capabilities through strategic inpainting-guided policy optimization. We utilize the 213 reasoning traces from the MetaMathQA dataset for the elastic inpainting process, creating effective 214 guidance signals that fit within our computational constraints. Detailed training hyperparameters are provided in Section F.



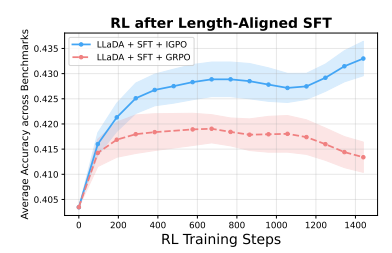


Figure 3: **RL** training curves of IGPO versus normal GRPO sampling. (a) Starting from LLaDA-8B-Instruct. (b) Starting from the *length-aligned* SFT checkpoint. IGPO exhibits superior and more stable training performance under both initialization checkpoints compared to standard GRPO sampling. Results are averaged over 3 random seeds across four mathematical reasoning benchmarks (GSM8K, MATH500, AMC and Minerva Math), with standard errors shown as shaded regions.

4.2 Experimental Setup

We conduct experiments using LLaDA-8B-Instruct as the base model with a sampling temperature of 1.2 for RL online generation, where the temperature is selected based on exploration and exploitation analysis detailed in Appendix F.1. For reinforcement learning, we train on the MetaMathQA dataset (Yu et al., 2023), specifically using the "Answer Augmentation" split and combining questions from both GSM8K and MATH500. After deduplicating identical questions, we obtain 12,794 unique training examples. For supervised fine-tuning, we utilize the OpenR1-Math-220K dataset with rewritten reasoning traces as described in Section 3.2. We evaluate our approach on four mathematics benchmarks: GSM8K (Cobbe et al., 2021), MATH500 (Hendrycks et al., 2021), AMC (LI et al., 2024) and Minerva Math (Lewkowycz et al., 2022). Experiments are conducted on 8×8 80GB H100 GPUs. For UniGRPO (Yang et al., 2025) baseline, we reproduce based on their Algorithm 1. We provide detailed experiment hyperparameter setups in Section F and Section H.

4.3 Main Results

Table 1: Performance across multiple mathematics tasks. GSM8K, MATH500 and Minerva are evaluated with pass@1 at temperature of 0.0, and AMC with avg@16 at temperature 0.1. Underlined scores indicate the best *within each initialization group*. Parenthesized deltas typeset via (+) denote absolute percentage-point improvements *relative to the LLaDA-8B-Instruct* baseline.

Model	GSM8K (pass@1)	MATH500 (pass@1)	AMC (avg@16)	Minerva (pass@1)	Average
Similar-size	d autoregress	sive LLMs			
LLaMA3-8B (AI@Meta, 2024)	79.6	30.0	_	_	-
Qwen2.5-7B (Team, 2024)	85.4	49.8	_	=	=
Prior ma.	sked dLLM be	aselines			
Dream-7B (Ye et al., 2025)	77.2	39.6	_	_	_
d1-LLaDA (Zhao et al., 2025)	82.1	40.2	_	_	_
wd1 (Tang et al., 2025)	82.3	39.0	_	_	_
LLaDA-1.5 (Zhu et al., 2025)	83.3	42.6	13.6	8.8	37.1
LLaDA-Instruct (Nie et al., 2025)	81.5(+0)	$39.0 (\pm 0)$	$14.5 (\pm 0)$	$9.2 (\pm 0)$	$36.0 (\pm 0)$
RL from	m LLaDA-Ins	truct			
LLaDA-Instruct + UniGRPO (Yang et al., 2025)	82.2(+0.7)	39.2 (+0.2)	15.0(+0.5)	11.0(+1.8)	36.9 (+0.9)
LLaDA-Instruct + DiffuGRPO (Zhao et al., 2025)	82.4(+0.9)	40.2 (+1.2)	15.5(+1.0)	10.3 (+1.1)	37.1 (+1.1)
LLaDA-Instruct + IGPO (ours)	83.1 (+1.6)	42.8(+3.8)	<u>17.5</u> (+3.0)	12.1(+2.9)	38.9 (+2.9)
Length-aligned SFT on LLaD	A-Instruct an	d RL on the SF	T checkpoint		
LLaDA-Instruct + Length-aligned SFT (ours)	83.6(+2.1)	45.2 (+6.2)	22.3 (+7.8)	10.3 (+1.1)	40.4 (+4.4)
LLaDA-Instruct + Length-aligned SFT + IGPO (ours)	86.8 (+5.3)	47.4 (+8.4)	25.9 (+11.4)	13.2 (+4.0)	43.3 (+7.3)

As shown in Table 1, our training recipe demonstrates consistent improvements across all mathematical reasoning benchmarks. With *Length-Aligned* SFT on rewritten traces, LLaDA achieves an average improvement of 4.4% compared to the base LLaDA-8B-Instruct model. When applying IGPO on top of the SFT model, we observe additional improvements, resulting in a total average improvement of 7.3%. The complete two-stage pipeline yields cumulative improvements of 5.3% on

GSM8K, 8.4% on MATH500, 11.4% on AMC, and 4.0% on Minerva relative to the LLaDA-Instruct baseline. Notably, on the challenging AMC benchmark, our approach achieves 25.9% (avg@16). As shown in Figure 3, IGPO exhibits superior training dynamics compared to standard GRPO sampling when initializing from before or after SFT. IGPO effectively reduces the all-wrong group ratio by approximately 60%, as shown in Figure 1(b). Our final model (LLaDA + *Length-Aligned* SFT + IGPO) outperforms all baseline approaches including the recent LLaDA-1.5 model across all evaluated benchmarks. Notably, even without SFT, applying IGPO directly on LLaDA achieves better performance than the previous LLaDA-1.5 and other RL methods for full-attention dLLMs, establishing a new state-of-the-art recipe for mathematical reasoning in masked diffusion language models.

4.4 Analysis and Ablation Studies

Self-generated inpainted traces provide better learning signal than ground truth traces.

The results in Figure 4 show that partial hint injection achieves higher performance than full hint injection. When the hint injection ratio varies within the lower range, the model needs to generate self-rationalized inpainting traces (with an example shown in Section G), and only those that lead to correct solutions are added to the group for gradient updates. Through inpainting, the model attempts to coherently connect provided hint chunks with its own reasoning steps. The inpainted generation produces a learning signal that bridges the gap between the model's current capabilities and the target behavior. The self-generated portions reflect the model's current reasoning patterns and are more "on-policy" while incorporating structural guidance from ground truth chunks, resulting in more effective policy optimization compared to pure supervised learning, reducing the distributional mismatch. This bridging of SFT and online RL through partial self-generation leads to more effective policy optimization.

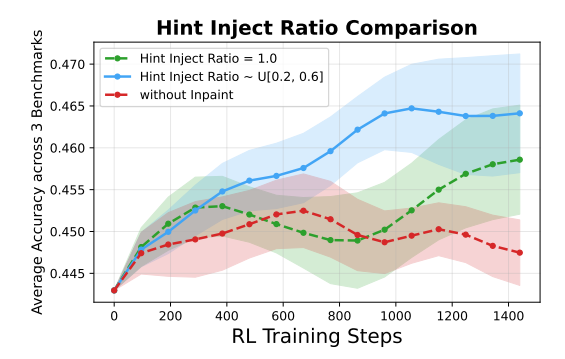


Figure 4: **Impact of hint injection ratio.** across 3 datasets (GSM8K, MATH500 and AMC) and 3 seeds with standard error shown as shaded areas. We compare partial hint injection ($\eta \sim \mathcal{U}[0.2, 0.6]$) versus full hint injection ($\eta = 1.0$). Partial hint injection consistently outperforms full hint injection, demonstrating the benefits of self-generated reasoning. Both hint-guided inpainting variants outperform the baseline without any hint injection.

Entropy clipping prevents training instability from off-policy tokens. As shown in Figure 5a, we observe that learning from only the top 20% highest-entropy hint token positions ($\tau=0.2$) achieves the best performance and exhibits the most stable training dynamics. In contrast, learning from all hint token positions ($\tau=1.0$) or a large fraction ($\tau=0.8$) leads to more unstable training with performance fluctuations compared to lower values like 0.2. This empirical finding supports our motivation that restricting gradient updates to high-entropy positions prevents the destabilizing effects of large gradients on high-entropy positions. The validates the necessity of entropy-based filtering when incorporating ground truth traces from hint-guided inpainting into policy gradient training.

Effect of reasoning trace rewriting for SFT and subsequent RL training. The results in Figure 5b illustrate two key findings. First, SFT on rewritten reasoning traces produces substantially stronger checkpoints than SFT on the original traces. Our rewritten traces eliminate verbose reflection behaviors and compress reasoning into concise trajectories (up to 1024 tokens), which are better aligned with LLaDA's generation budget (256 tokens) and evaluation sequence length. This alignment improves SFT accuracy at step 0 relative to models trained on the longer 4096-token traces. Second, while RL training can partially compensate for weaker SFT checkpoints—the models trained on 4096-token traces recover accuracy rapidly in early RL steps—starting from stronger rewritten SFT checkpoints leads to consistently higher final performance. Importantly, across both initialization settings, IGPO outperforms standard RL without inpainting. Additionally, IGPO preserves output diversity and stabilizes pass@5 performance throughout training, whereas standard GRPO exhibits a decline in pass@k metrics, indicative of reduced exploration and mode collapse.

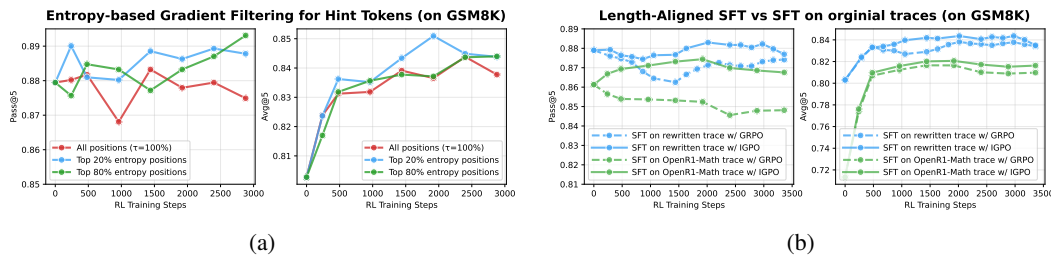


Figure 5: (a) Impact of entropy clipping threshold on hint tokens. Performance comparison across different entropy clipping thresholds τ applied to hint token positions in IGPO, where $\tau=0.2$ represents learning from only the top 20% highest-entropy hint token positions, while $\tau=1.0$ indicates learning from all hint token positions without filtering. (b) SFT and RL dynamics with rewritten vs. original traces. We compare models fine-tuned on concise rewritten traces (max 1024 tokens) vs on original OpenR1-Math traces truncated at LLaDA's 4096 context limit. RL is then applied (GRPO or IGPO) to both models. Rewritten traces yield stronger SFT performance and superior RL outcomes. IGPO consistently outperforms GRPO with stable pass@5 while GRPO suffers from diversity collapse. Results are run on GSM8K with temperature 0.1 and length 256.

Elastic inpainting outperforms sequential SFT and GRPO We further validate the effectiveness of our elastic inpainting approach by comparing it against sequentially performing SFT on the RL dataset's reasoning traces followed by standard GRPO (see Section E for details). This ablation confirms that IGPO's elastic hint injection during zero-advantage scenarios is superior to uniformly applying SFT on concise reasoning traces across all prompts before applying GRPO. The uniform SFT approach can degrade initial performance due to distribution shift in reasoning patterns, whereas injecting partial hints allows dLLMs to inpaint longer, more "on-policy" reasoning traces.

5 Related Work

Diffusion Language Models: Recent advances in diffusion language models have progressed from continuous approaches mapping discrete text to continuous representations (Chen et al., 2022; Li et al., 2022; Gong et al., 2023) to scaled discrete diffusion models, with masked diffusion emerging as a prominent approach (Austin et al., 2021; Sahoo et al., 2024; Shi et al., 2024; Ou et al., 2024; Nie et al., 2024). Notable developments include DiffuLLaMA (Gong et al., 2025a) and Dream (Ye et al., 2025) adapted from pretrained autoregressive LLMs, and LLaDA (Nie et al., 2025) as a masked diffusion LLM trained from scratch achieving comparable performance to autoregressive models. Commercial models like Mercury (Inception Labs et al., 2025) and Gemini Diffusion (DeepMind, 2025) have demonstrated practical viability with significantly faster inference. **Reinforcement Learning for Diffusion Language Models:** Applying RL to diffusion LLMs faces unique challenges due to intractable likelihood estimation, which is required for policy optimization. Recent solutions include diffu-GRPO (Zhao et al., 2025) with mean-field approximation, MMaDA (Yang et al., 2025) and coupled-GRPO (Gong et al., 2025b) with improved masking strategies, LLaDA 1.5 (Zhu et al., 2025) addressing variance through preference optimization, wd1 (Tang et al., 2025) eliminating policy ratios via weighted likelihood objectives, and SDPO (Han et al., 2025) decomposing trajectory alignment into stepwise subproblems. More detailed related works are discussed in Section C.

6 Conclusion

We introduced IGPO, a reinforcement learning algorithm that leverages the inpainting capabilities of masked diffusion language models. By injecting ground-truth reasoning hints during denoising, IGPO steers the policy toward high-reward regions and alleviates the exploration bottleneck in RL. It resolves the zero-advantage dilemma by inducing reward variance that supports effective policy gradient updates when standard sampling yields uniform outcomes. To further strengthen RL initialization, we proposed *Length-Aligned* SFT, which reduces the length mismatch across SFT, RL, and evaluation stages. Combined with entropy-based gradient filtering, our approach achieves new state-of-the-art performance among full-attention masked dLLMs on multiple mathematical reasoning benchmarks. These results highlight a new paradigm for reinforcement learning in masked diffusion language models, showing how architectural properties can be systematically exploited to address critical optimization challenges.

References

- Arash Ahmadian, Chris Cremer, Matthias Gallé, Marzieh Fadaee, Julia Kreutzer, Olivier Pietquin,
 Ahmet Üstün, and Sara Hooker. Back to basics: Revisiting reinforce style optimization for learning
 from human feedback in Ilms. *arXiv preprint arXiv:2402.14740*, 2024.
- AI@Meta. Llama 3 model card. 2024. https://github.com/meta-llama/llama3/blob/mai n/MODEL_CARD.md.
- Chenxin An, Zhihui Xie, Xiaonan Li, Lei Li, Jun Zhang, Shansan Gong, Ming Zhong, Jingjing Xu, Xipeng Qiu, Mingxuan Wang, and Lingpeng Kong. Polaris: A post-training recipe for scaling reinforcement learning on advanced reasoning models, 2025. https://hkunlp.github.io/blog/2025/Polaris.
- Marianne Arriola, Aaron Gokaslan, Justin T Chiu, Zhihan Yang, Zhixuan Qi, Jiaqi Han, Subham Sekhar Sahoo, and Volodymyr Kuleshov. Block diffusion: Interpolating between autoregressive and diffusion language models. In *The Thirteenth International Conference on Learning Representations*, 2025.
- Jacob Austin, Daniel D Johnson, Jonathan Ho, Daniel Tarlow, and Rianne Van Den Berg. Structured
 denoising diffusion models in discrete state-spaces. *Advances in neural information processing* systems, 34:17981–17993, 2021.
- Yuntao Bai, Andy Jones, Kamal Ndousse, Amanda Askell, Anna Chen, Nova DasSarma, Dawn Drain,
 Stanislav Fort, Deep Ganguli, Tom Henighan, et al. Training a helpful and harmless assistant with
 reinforcement learning from human feedback. *arXiv preprint arXiv:2204.05862*, 2022.
- Ting Chen, Ruixiang Zhang, and Geoffrey E. Hinton. Analog bits: Generating discrete data using diffusion models with self-conditioning. *ArXiv*, abs/2208.04202, 2022.
- Karl Cobbe, Vineet Kosaraju, Mohammad Bavarian, Mark Chen, Heewoo Jun, Lukasz Kaiser,
 Matthias Plappert, Jerry Tworek, Jacob Hilton, Reiichiro Nakano, et al. Training verifiers to solve
 math word problems. *arXiv preprint arXiv:2110.14168*, 2021.
- DeepMind. Gemini diffusion, 2025. https://deepmind.google/models/gemini-diffusion/.
- Shansan Gong, Mukai Li, Jiangtao Feng, Zhiyong Wu, and Lingpeng Kong. DiffuSeq: Sequence to sequence text generation with diffusion models. In *International Conference on Learning Representations, ICLR*, 2023.
- Shansan Gong, Shivam Agarwal, Yizhe Zhang, Jiacheng Ye, Lin Zheng, Mukai Li, Chenxin An, Peilin Zhao, Wei Bi, Jiawei Han, Hao Peng, and Lingpeng Kong. Scaling diffusion language models via adaptation from autoregressive models. In *The Thirteenth International Conference on Learning Representations*, 2025a.
- Shansan Gong, Huangjie Zheng Ruixiang Zhang, Jiatao Gu, Navdeep Jaitly, Lingpeng Kong, and Yizhe Zhang. Diffucoder: Understanding and improving masked diffusion models for code generation. 2025b. https://arxiv.org/abs/2506.20639.
- Daya Guo, Dejian Yang, Haowei Zhang, Junxiao Song, Ruoyu Zhang, Runxin Xu, Qihao Zhu,
 Shirong Ma, Peiyi Wang, Xiao Bi, et al. Deepseek-r1: Incentivizing reasoning capability in llms
 via reinforcement learning. *arXiv preprint arXiv:2501.12948*, 2025.
- Jiaqi Han, Austin Wang, Minkai Xu, Wenda Chu, Meihua Dang, Yisong Yue, and Stefano Ermon.
 Discrete diffusion trajectory alignment via stepwise decomposition, 2025. https://arxiv.org/abs/2507.04832.
- Dan Hendrycks, Collin Burns, Saurav Kadavath, Akul Arora, Steven Basart, Eric Tang, Dawn Song, and Jacob Steinhardt. Measuring mathematical problem solving with the math dataset. *arXiv* preprint arXiv:2103.03874, 2021.
- Zhanqiu Hu, Jian Meng, Yash Akhauri, Mohamed S. Abdelfattah, Jae sun Seo, Zhiru Zhang, and
 Udit Gupta. Accelerating diffusion language model inference via efficient kv caching and guided
 diffusion, 2025. https://arxiv.org/abs/2505.21467.

- Zeyu Huang, Tianhao Cheng, Zihan Qiu, Zili Wang, Yinghui Xu, Edoardo M. Ponti, and Ivan
 Titov. Blending supervised and reinforcement fine-tuning with prefix sampling, 2025. https://arxiv.org/abs/2507.01679.
- Inception Labs, Samar Khanna, Siddhant Kharbanda, Shufan Li, Harshit Varma, Eric Wang, Sawyer
 Birnbaum, Ziyang Luo, Yanis Miraoui, Akash Palrecha, Stefano Ermon, Aditya Grover, and
 Volodymyr Kuleshov. Mercury: Ultra-fast language models based on diffusion. 2025. https://arxiv.org/abs/2506.17298.
- Daniel Israel, Guy Van den Broeck, and Aditya Grover. Accelerating diffusion llms via adaptive parallel decoding, 2025. https://arxiv.org/abs/2506.00413.
- Aitor Lewkowycz, Anders Johan Andreassen, David Dohan, Ethan Dyer, Henryk Michalewski,
 Vinay Venkatesh Ramasesh, Ambrose Slone, Cem Anil, Imanol Schlag, Theo Gutman-Solo, Yuhuai
 Wu, Behnam Neyshabur, Guy Gur-Ari, and Vedant Misra. Solving quantitative reasoning problems
 with language models. In Alice H. Oh, Alekh Agarwal, Danielle Belgrave, and Kyunghyun Cho,
 editors, Advances in Neural Information Processing Systems, 2022. https://openreview.net/forum?id=IFXTZERXdM7.
- Jia LI, Edward Beeching, Lewis Tunstall, Ben Lipkin, Roman Soletskyi, Shengyi Costa Huang,
 Kashif Rasul, Longhui Yu, Albert Jiang, Ziju Shen, Zihan Qin, Bin Dong, Li Zhou, Yann Fleureau,
 Guillaume Lample, and Stanislas Polu. Numinamath. https://github.com/project-numin
 a/aimo-progress-prize/blob/main/report/numina_dataset.pdf, 2024.
- Shufan Li, Konstantinos Kallidromitis, Hritik Bansal, Akash Gokul, Yusuke Kato, Kazuki Kozuka,
 Jason Kuen, Zhe Lin, Kai-Wei Chang, and Aditya Grover. Lavida: A large diffusion language
 model for multimodal understanding. *ArXiv preprint*, abs/2505.16839, 2025. https://arxiv.org/abs/2505.16839.
- Xiang Lisa Li, John Thickstun, Ishaan Gulrajani, Percy Liang, and Tatsunori Hashimoto. Diffusion-lm improves controllable text generation. *ArXiv*, abs/2205.14217, 2022.
- Ziniu Li, Tian Xu, Yushun Zhang, Zhihang Lin, Yang Yu, Ruoyu Sun, and Zhi-Quan Luo. Remax: A
 simple, effective, and efficient reinforcement learning method for aligning large language models.
 arXiv preprint arXiv:2310.10505, 2023.
- Zhiyuan Liu, Yicun Yang, Yaojie Zhang, Junjie Chen, Chang Zou, Qingyuan Wei, Shaobo Wang, and
 Linfeng Zhang. dllm-cache: Accelerating diffusion large language models with adaptive caching.
 arXiv preprint arXiv:2506.06295, 2025a.
- Zichen Liu, Changyu Chen, Wenjun Li, Penghui Qi, Tianyu Pang, Chao Du, Wee Sun Lee, and Min
 Lin. Understanding r1-zero-like training: A critical perspective. arXiv preprint arXiv:2503.20783,
 2025b.
- Aaron Lou, Chenlin Meng, and Stefano Ermon. Discrete diffusion modeling by estimating the ratios of the data distribution. In *Forty-first International Conference on Machine Learning*, 2024.
- Xinyin Ma, Runpeng Yu, Gongfan Fang, and Xinchao Wang. dkv-cache: The cache for diffusion language models, 2025. https://arxiv.org/abs/2505.15781.
- AI Meta. The llama 4 herd: The beginning of a new era of natively multimodal ai innovation. https://ai. meta. com/blog/llama-4-multimodal-intelligence/, 2025.
- Jinjie Ni and the team. Diffusion language models are super data learners. https://jinjieni.n otion.site/Diffusion-Language-Models-are-Super-Data-Learners-239d8f03a86 6800ab196e49928c019ac, 2025. Notion Blog.
- Shen Nie, Fengqi Zhu, Chao Du, Tianyu Pang, Qian Liu, Guangtao Zeng, Min Lin, and Chongxuan Li. Scaling up masked diffusion models on text. *arXiv preprint arXiv:2410.18514*, 2024.
- Shen Nie, Fengqi Zhu, Zebin You, Xiaolu Zhang, Jingyang Ou, Jun Hu, Jun Zhou, Yankai Lin, Ji-Rong Wen, and Chongxuan Li. Large language diffusion models, 2025. https://arxiv.org/abs/2502.09992.

- Jingyang Ou, Shen Nie, Kaiwen Xue, Fengqi Zhu, Jiacheng Sun, Zhenguo Li, and Chongxuan Li.
 Your absorbing discrete diffusion secretly models the conditional distributions of clean data. *arXiv*preprint arXiv:2406.03736, 2024.
- Long Ouyang, Jeffrey Wu, Xu Jiang, Diogo Almeida, Carroll Wainwright, Pamela Mishkin, Chong
 Zhang, Sandhini Agarwal, Katarina Slama, Alex Ray, et al. Training language models to follow
 instructions with human feedback. Advances in neural information processing systems, 35:27730–
 27744, 2022.
- Mihir Prabhudesai, Mengning Wu, Amir Zadeh, Katerina Fragkiadaki, and Deepak Pathak. Diffusion beats autoregressive in data-constrained settings, 2025. https://arxiv.org/abs/2507.15857.
- Subham S. Sahoo, Marianne Arriola, Yair Schiff, Aaron Gokaslan, Edgar Marroquin, Justin T. Chiu,
 Alexander Rush, and Volodymyr Kuleshov. Simple and effective masked diffusion language models.
 In Amir Globersons, Lester Mackey, Danielle Belgrave, Angela Fan, Ulrich Paquet, Jakub M.
 Tomczak, and Cheng Zhang, editors, Advances in Neural Information Processing Systems 38:
 Annual Conference on Neural Information Processing Systems 2024, NeurIPS 2024, Vancouver,
 BC, Canada, December 10 15, 2024, 2024. http://papers.nips.cc/paper_files/paper
 /2024/hash/eb0b13cc515724ab8015bc978fdde0ad-Abstract-Conference.html.
- Subham Sekhar Sahoo, Zhihan Yang, Yash Akhauri, Johnna Liu, Deepansha Singh, Zhoujun Cheng,
 Zhengzhong Liu, Eric Xing, John Thickstun, and Arash Vahdat. Esoteric language models, 2025.
 https://arxiv.org/abs/2506.01928.
- John Schulman, Filip Wolski, Prafulla Dhariwal, Alec Radford, and Oleg Klimov. Proximal policy optimization algorithms. *arXiv preprint arXiv:1707.06347*, 2017.
- Zhihong Shao, Peiyi Wang, Qihao Zhu, Runxin Xu, Junxiao Song, Xiao Bi, Haowei Zhang, Mingchuan Zhang, YK Li, Y Wu, et al. Deepseekmath: Pushing the limits of mathematical reasoning in open language models. *arXiv preprint arXiv:2402.03300*, 2024.
- Jiaxin Shi, Kehang Han, Zhe Wang, Arnaud Doucet, and Michalis K. Titsias. Simplified and generalized masked diffusion for discrete data. In Amir Globersons, Lester Mackey, Danielle Belgrave, Angela Fan, Ulrich Paquet, Jakub M. Tomczak, and Cheng Zhang, editors, Advances in Neural Information Processing Systems 38: Annual Conference on Neural Information Processing Systems 2024, NeurIPS 2024, Vancouver, BC, Canada, December 10 15, 2024, 2024. http://papers.nips.cc/paper_files/paper/2024/hash/bad233b9849f019aead5e5cc60cef70f-Abstract-Conference.html.
- Xiaohang Tang, Rares Dolga, Sangwoong Yoon, and Ilija Bogunovic. wd1: Weighted policy
 optimization for reasoning in diffusion language models, 2025. https://arxiv.org/abs/2507
 .08838.
- Kimi Team, Angang Du, Bofei Gao, Bowei Xing, Changjiu Jiang, Cheng Chen, Cheng Li, Chenjun
 Xiao, Chenzhuang Du, Chonghua Liao, et al. Kimi k1. 5: Scaling reinforcement learning with
 llms. arXiv preprint arXiv:2501.12599, 2025.
- Qwen Team. Qwen2.5: A party of foundation models, September 2024. https://qwenlm.github.io/blog/qwen2.5/.
- Chengyue Wu, Hao Zhang, Shuchen Xue, Zhijian Liu, Shizhe Diao, Ligeng Zhu, Ping Luo, Song
 Han, and Enze Xie. Fast-dllm: Training-free acceleration of diffusion llm by enabling kv cache
 and parallel decoding, 2025. https://arxiv.org/abs/2505.22618.
- Ling Yang, Ye Tian, Bowen Li, Xinchen Zhang, Ke Shen, Yunhai Tong, and Mengdi Wang. Mmada:
 Multimodal large diffusion language models. *ArXiv preprint*, abs/2505.15809, 2025. https://arxiv.org/abs/2505.15809.
- Jiacheng Ye, Zhihui Xie, Lin Zheng, Jiahui Gao, Zirui Wu, Xin Jiang, Zhenguo Li, and Lingpeng Kong. Dream 7b, 2025. https://hkunlp.github.io/blog/2025/dream.
- Zebin You, Shen Nie, Xiaolu Zhang, Jun Hu, Jun Zhou, Zhiwu Lu, Ji-Rong Wen, and Chongxuan
 Li. Llada-v: Large language diffusion models with visual instruction tuning. arXiv preprint
 arXiv:2505.16933, 2025.

- Longhui Yu, Weisen Jiang, Han Shi, Jincheng Yu, Zhengying Liu, Yu Zhang, James T Kwok, Zhenguo Li, Adrian Weller, and Weiyang Liu. Metamath: Bootstrap your own mathematical questions for large language models. *arXiv preprint arXiv:2309.12284*, 2023.
- Wenhao Zhang, Yuexiang Xie, Yuchang Sun, Yanxi Chen, Guoyin Wang, Yaliang Li, Bolin Ding, and Jingren Zhou. On-policy rl meets off-policy experts: Harmonizing supervised fine-tuning and reinforcement learning via dynamic weighting, 2025. https://arxiv.org/abs/2508.11408.
- Siyan Zhao, Devaansh Gupta, Qinqing Zheng, and Aditya Grover. d1: Scaling reasoning in diffusion large language models via reinforcement learning. *arXiv preprint arXiv:2504.12216*, 2025.
- Chujie Zheng, Shixuan Liu, Mingze Li, Xiong-Hui Chen, Bowen Yu, Chang Gao, Kai Dang,
 Yuqiong Liu, Rui Men, An Yang, et al. Group sequence policy optimization. arXiv preprint
 arXiv:2507.18071, 2025.
- Fengqi Zhu, Rongzhen Wang, Shen Nie, Xiaolu Zhang, Chunwei Wu, Jun Hu, Jun Zhou, Jianfei Chen, Yankai Lin, Ji-Rong Wen, and Chongxuan Li. Llada 1.5: Variance-reduced preference optimization for large language diffusion models. *ArXiv preprint*, abs/2505.19223, 2025. https://arxiv.org/abs/2505.19223.

487 A Use of Large Language Models Disclosure

LLMs were used only for minor editing (grammar and phrasing) and to generate speech narration for the supplementary presentation video from an author-written script. All research ideas, methods, experiments, analyses, and substantive writing were carried out by the authors without LLM assistance.

492 B Preliminaries

493

494

495

496

497

498

499

500

501

502

503

504

505

506

516

B.1 Masked Diffusion Large Language Models

Masked diffusion LLMs (Austin et al., 2021; Sahoo et al., 2024; Shi et al., 2024; Ou et al., 2024; Lou et al., 2024) employ a forward diffusion process that progressively corrupts token sequences x_0 through introduction of mask tokens. This corruption process is parameterized by time $t \in [0, 1]$. At any given timestep t, the resulting sequence x_t contains partial masking, where each token maintains a probability α_t of remaining unmasked. The noise schedule α_t exhibits strict monotonic decrease with respect to t. Complete masking occurs at t=1, where all tokens in x_1 become masked. The training procedure for masked dLLMs follows a forward process through definition of α_t and a bidirectional unmasking predictor f_{θ} with learnable parameters. During each training step, we stochastically sample timestep $t \in [0,1)$ and apply token masking according to the designated forward process. Given these corrupted sequences, the training objective seeks to recover the original tokens. The standard optimization criterion employs the negative evidence lower bound (NELBO), which provides an upper bound for the negative log-likelihood (NLL) of the training data. For masked dLLMs, this NELBO reduces to a weighted NLL formulation, with weighting coefficients derived from transformations of α_t (Sahoo et al., 2024, Equation (10)). For example, LLaDA (Nie et al., 2025) specifies the forward process through $\alpha_t = 1 - t$, yielding the following NELBO formulation:

$$-\mathbb{E}_{t \sim \mathcal{U}[0,1), \ x_0 \sim p_{\text{data}}, \ x_t \sim q_{t|0}(x_t|x_0)} \left[\frac{1}{t} \sum_{k=1}^{|x_t|} \mathbb{1}[x_t^k = \text{mask}] \log f_{\theta}(x_0^k \mid x_t) \right], \tag{6}$$

where $|x_t|$ denotes the sequence length of x, and x^k represents the k-th token position. The loss computation is restricted to tokens masked at timestep t.

During prompt conditional generation, the model starts with a sequence where prompt tokens remain unmasked and continuation tokens are initially masked, then progressively unmasks the continuation tokens through ancestral sampling from the reverse process $p_{\theta}(x_s \mid x_t)$ for timesteps t > s, where the model f_{θ} provides the denoising predictions for masked positions. The reverse process maintains the property that unmasked tokens are carried over unchanged throughout all denoising steps.

B.2 Policy Optimization for Masked Diffusion Large Language Models

Policy-gradient methods have gained widespread adoption for post-training LLMs (Ouyang et al., 2022; Bai et al., 2022; Li et al., 2023; Ahmadian et al., 2024). Online RL—particularly Group Relative Policy Optimization (GRPO)—has proved effective for improving language models (Shao et al., 2024; Guo et al., 2025; Team et al., 2025). GRPO (Shao et al., 2024) offers a computationally efficient alternative to PPO (Schulman et al., 2017) by using group-based statistics for advantage estimation, avoiding separate value-function training.

The GRPO objective integrates clipping for stability and reverse KL regularization:

$$\mathcal{L}_{\text{GRPO}}(\theta) = \mathbb{E}_{\substack{q \sim \mathcal{D} \\ o_1, \dots, o_G \sim \pi_{\theta_{\text{old}}}(\cdot|q)}} \left[\frac{1}{G} \sum_{i=1}^{G} \frac{1}{|o_i|} \sum_{k=1}^{|o_i|} \min\left(\rho_i^k A_i, \text{clip}\left(\rho_i^k, 1 - \varepsilon, 1 + \varepsilon\right) A_i\right) - \beta D_{\text{KL}}\left[\pi_{\theta}(\cdot|q) \| \pi_{\text{ref}}(\cdot|q)\right] \right], \quad (7)$$

where $\rho_i^k = \frac{\pi_{\theta}(o_i^k|q,o_i^{< k})}{\pi_{\theta_{\text{old}}}(o_i^k|q,o_i^{< k})}$ is the likelihood ratio.

For a query q, GRPO samples G responses $\{o_1,\ldots,o_G\}$ from the behavior policy $\pi_{\theta_{\text{old}}}$ and assigns a single sequence-level advantage per response. Following Liu et al. (2025b), we use the unnormalized group-relative advantage $A_i = r(o_i) - \frac{1}{G} \sum_{j=1}^G r(o_j)$, where r is the reward function. This scalar A_i is shared by all tokens in o_i when forming the tokenwise objective.

Applying Policy Gradient Methods to Diffusion LLMs Applying GRPO to dLLMs is nontrivial. The objective in Equation (7) requires (i) *token-level* probabilities for importance ratios and (ii) *sequence-level* probabilities for KL regularization. Autoregressive models provide per-token conditionals via sequential factorization, enabling one-pass sequence scoring by the chain rule: $\log \pi_{AR}(o \mid q) = \sum_{k=1}^{|o|} \log \pi_{AR}(o^k \mid q, o^{< k})$. Accordingly, the reverse-KL decomposes as

$$D_{\mathrm{KL}}\left[\pi_{\theta}(\cdot \mid q) \mid \mid \pi_{\mathrm{ref}}(\cdot \mid q)\right] = \mathbb{E}_{o \sim \pi_{\theta}(\cdot \mid q)} \left[\sum_{k=1}^{|o|} \log \frac{\pi_{\theta}(o^k \mid q, o^{< k})}{\pi_{\mathrm{ref}}(o^k \mid q, o^{< k})} \right]. \tag{8}$$

In contrast, dLLMs do not admit a sequential factorization of $\pi(o \mid q)$. dLLM's generation invokes the unmasking predictor f_{θ} across M denoising steps, making π_{θ} a composition of M mappings. Exact tokenwise probabilities would require marginalization over denoising trajectories and maintaining (and differentiating through) full denoising trajectories, which is computationally prohibitive. To address this, recent work develops efficient approximations for policy optimization in masked diffusion LLMs. DiffuGRPO (Zhao et al., 2025) employs a mean-field approximation that yields single-pass estimates of both token-level and sequence-level terms, replacing explicit multi-step unrolling with a single-sample Monte Carlo estimate. While this introduces bias relative to the exact diffusion policy, it provides a practical framework for GRPO-style optimization on dLLMs. In our method, we adopt the mean-field estimators of Zhao et al. (2025) to compute the token-level importance ratios ρ_i^k and the reverse-KL term with one forward pass per policy.

C Related Work

535

536

537

538

539

542

543

545

546

547

548

549 550

552

553

554

555

556

557

558

560 561

562

563

565

566

567

568

569

571

572

573

574

C.1 Diffusion Language Models

Diffusion language models was first explored through continuous approaches that map discrete text to continuous representations, including learned embeddings, sequence-to-sequence conditioning, and binary bit representations (Chen et al., 2022; Li et al., 2022; Gong et al., 2023). Recently, discrete diffusion language models have been scaled up significantly, with masked diffusion established as a specific instance of discrete diffusion (Austin et al., 2021; Sahoo et al., 2024; Shi et al., 2024; Ou et al., 2024; Nie et al., 2024). Notable developments include DiffuLLaMA (Gong et al., 2025a) and Dream (Ye et al., 2025), both adapted from pretrained autoregressive LLMs. LLaDA (Nie et al., 2025) represents a breakthrough as a masked diffusion LLM trained from scratch using full-attention, achieving performance comparable to similarly-sized autoregressive models. These approaches are predominantly based on masked modeling. Unlike these full-attention dLLMs, Block Diffusion (Arriola et al., 2025) introduced a hybrid approach that models sequences block-by-block while applying diffusion within each block, enabling flexible length generation and improved inference efficiency through kv-caching. Recent commercial models like Mercury (Inception Labs et al., 2025) and Gemini Diffusion (DeepMind, 2025) have demonstrated the practical viability of diffusion-based code generation, achieving performance comparable to leading autoregressive models while offering significantly faster inference. More recent works have introduced caching and parallel decoding algorithms (Wu et al., 2025; Liu et al., 2025a; Ma et al., 2025; Israel et al., 2025; Sahoo et al., 2025; Hu et al., 2025) that significantly improve inference efficiency for masked diffusion language models. In this work, we focus on full-attention masked dLLMs.

C.2 Reinforcement Learning for Diffusion Language Models

Applying reinforcement learning to diffusion language models presents unique challenges compared to autoregressive models. The primary obstacle is the intractability of likelihood functions in diffusion models, which necessitates approximating response likelihoods for policy optimization. This requirement introduces computational overhead and potential bias, particularly when approximation errors occur in policy ratios used for importance sampling. d1 proposed diffu-GRPO (Zhao et al., 2025) which adopts an efficient approximation through mean-field approximation. MMaDA (Yang et al., 2025) and diffucoder's coupled-GRPO (Gong et al., 2025b) further improve the masking strategy in log probabilities estimation to achieve better learning efficiency. LLaDA 1.5 (Zhu et al., 2025) tackles the variance issues in ELBO-based likelihood estimates through preference optimization. Recently, wd1 (Tang et al., 2025) addresses these challenges by reformulating policy optimization as a weighted likelihood objective that eliminates the need for policy ratios. SDPO (Han et al., 2025)

decomposes the diffusion trajectory alignment problem into stepwise subproblems that align the posterior at each diffusion step. Our inpainting method can also be applicable to some of the above online RL methods.

Additionally, a closely related work in RL for AR LLMs is Prefix-RFT (Huang et al., 2025), which samples prefixes from demonstrations to guide online exploration, though this is limited to left-to-right sequential generation that does not leverage the bidirectional conditioning capabilities of diffusion LLMs.

D Length-Aligned SFT: SFT trace revision length distribution comparison

As illustrated in Figure 6, the original OpenR1-Math-220K dataset exhibits substantial token length diversity, with reasoning traces extending beyond 10,000 tokens while LLaDA's maximum context length is only 4096 tokens. Naively applying SFT on this dataset would result in many truncated sequences, and even for samples within the 4096-token limit, significant distribution mismatch persists across training phases—we use 256 tokens for RL sampling and 512 tokens for evaluation. Our rewriting using LLaMA-4-Maverick successfully constrains all traces to under 1500 tokens, creating alignment between SFT training, RL sampling, and evaluation phases. Additionally, while reflective behavior has been found helpful for LLaDA in prior work (Zhao et al., 2025), the excessive repeated reflective patterns in the original dataset are unsuitable for its constrained generation space. The rewriting process eliminates this redundancy while preserving essential reasoning structure.

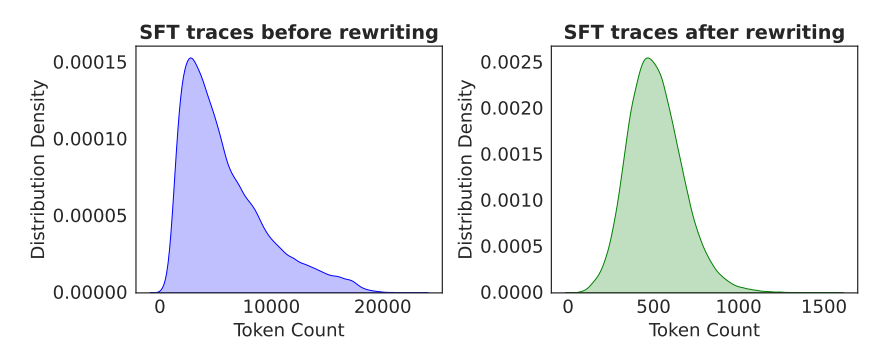


Figure 6: **Token Length Distribution of SFT Dataset Before and After Revision.** Comparison of token length distributions for the OpenR1-Math-220K dataset (94k math problems). After revision using LLaMA-4-Maverick, token lengths are constrained to below 1500 tokens, eliminating the extreme range of the original dataset where traces could exceed 20,000 tokens. This addresses the generation length mismatch across SFT training, RL sampling (256 tokens), and evaluation (512 tokens) phases.

E Ablation: SFT on hint traces then apply GRPO vs IGPO

In our RL training setup, we assume access to ground-truth reasoning traces for every query in the training dataset. To investigate whether direct supervised fine-tuning on these traces provides comparable benefits to our elastic inpainting approach, we conduct an ablation study comparing two strategies: (1) applying SFT on the RL dataset's reasoning traces followed by standard GRPO sampling, versus (2) directly applying IGPO with elastic hint injection only when all generated responses are incorrect.

Specifically, we first fine-tune the LLaDA-8B-Instruct model on the MetaMath dataset's reasoning traces for 20 epochs, then apply standard GRPO sampling. We compare this against our IGPO approach, which selectively injects partial reasoning hints from the same MetaMath dataset only when zero-advantage scenarios occur (i.e., when all sampled responses yield incorrect rewards).

The results in Figure 7 demonstrate that IGPO consistently outperforms the SFT-first variant. Notably, after SFT on the MetaMath dataset for 20 epochs, the model's initial performance drops significantly compared to the original LLaDA-8B-Instruct baseline. This degradation occurs because the MetaMath dataset contains very concise reasoning traces, many shorter than our 256-token generation length limit. Consequently, the model adopts overly concise reasoning patterns that prove insufficient for the challenging problems in our evaluation benchmarks (such as AMC and Minerva).

While subsequent RL training can recover performance to some extent—as evidenced by the rapid improvement in early training steps—it ultimately fails to match the effectiveness of IGPO. This comparison highlights two key advantages of our approach: (1) the effectiveness of applying inpainting guidance selectively only when the model struggles with specific queries, rather than forcing a uniform reasoning style through SFT, and (2) the critical importance of reducing all-wrong group occurrences, which successfully recovers gradient signals from otherwise degenerate zero-advantage scenarios.

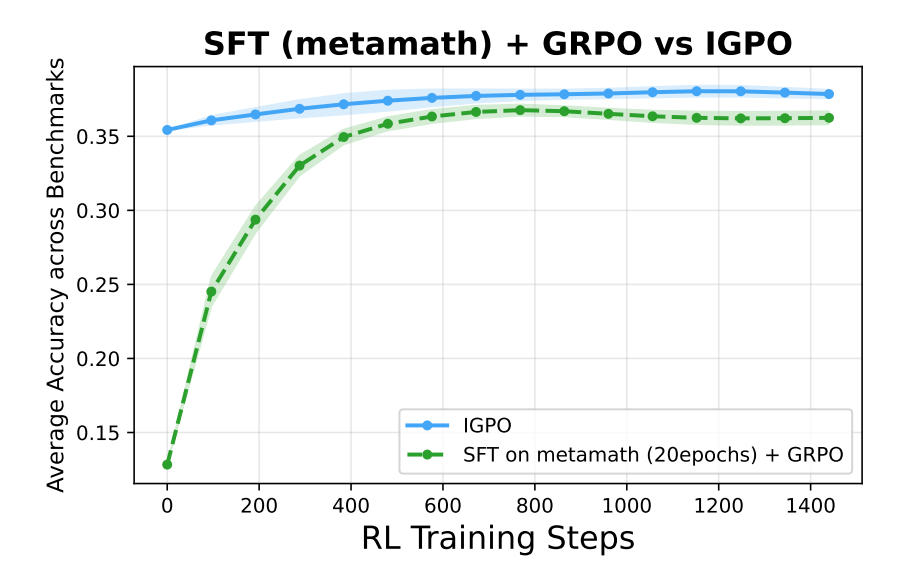


Figure 7: Comparison of SFT-first approach versus direct IGPO application. The SFT-first strategy involves fine-tuning on MetaMath reasoning traces for 20 epochs followed by standard GRPO, while IGPO applies inpainting-guided exploration elastically only during zero-advantage scenarios. IGPO demonstrates superior and more stable performance, avoiding the performance degradation caused by overly concise reasoning patterns learned during SFT on short traces. Results are averaged across four mathematical reasoning benchmarks with standard errors shown as shaded regions.

F Experiments Hyperparameters

Table 2: Training Hyperparameters

Table 2. Training Tryperparameter							
Parameter	Value						
SFT Training Parameters							
Per Device Train Batch Size	4						
Hardware Configuration	8×8 H100 GPUs						
Gradient Accumulation Steps	8						
Learning Rate	5×10^{-6}						
LR Schedule	Warmup-stable-decay						
LR Warmup Steps	200						
LR Min Value	1×10^{-6}						
LR Decay Period	Final 10% of steps						
Number of Epochs	100						
RL Sampling Parameters							
RL Online Sampling Generation Length L	256						
Diffusion Steps	128						
Block Length	32						
Sampling Temperature	1.2						
Generations Per Group G	8						
RL Training Parameters							
Per Device Train Batch Size	8						
Hardware Configuration	$8 \times 8 \text{ H}100 \text{ GPUs}$						
Gradient Accumulation Steps	1						
Effective Batch Size	512						
KL Beta β	0.01						
Policy Gradient Inner Iterations per Generation μ	4						
Learning Rate	5×10^{-7}						
LR Schedule	Linear decay to 0						
LR Warmup Steps	50						
LR Decay Period	10 epochs						
Training Steps	1440						
Clip Ratio Epsilon ε	0.2						
IGPO Specific Parameters	IGPO Specific Parameters						
Chunk Size $ c_j \sim \mathcal{U}[s_{\min}, s_{\max}]$	$\mathcal{U}[5,10]$						
Inpainting Ratio $\eta_i \sim \mathcal{U}[\eta_{\mathrm{low}}, \eta_{\mathrm{high}}]$	$\mathcal{U}[0.2, 0.6]$						
replacement fraction λ	0.5						
Entropy-based Gradient Filtering for Inpainted Tokens $ au$	0.2						

F.1 Temperature Selection for RL Training

Following the methodology established by Polaris An et al. (2025) for scaling reinforcement learning on advanced reasoning models, we conduct a systematic analysis to determine the optimal sampling temperature for our RL training process. We evaluate our model's performance across different sampling temperatures by analyzing both Pass@5 and Average@5 scores on the MATH500 dataset. We also divide three temperature regions: low temperatures (≤ 0.8) yield high accuracy but reduced diversity in generated rollouts, restricting the model's ability to explore diverse reasoning paths; high temperatures (≥ 1.6) preserve rollout diversity but significantly degrade accuracy due to increased noise in token generation; and the middle Controlled Exploration Zone (0.9-1.5) provides the optimal trade-off between maintaining reasonable accuracy and achieving sufficient diversity for effective RL training. Based on this analysis, we select temperature T=1.2 to balance exploration with sample quality and provide sufficient diversity for RL training.

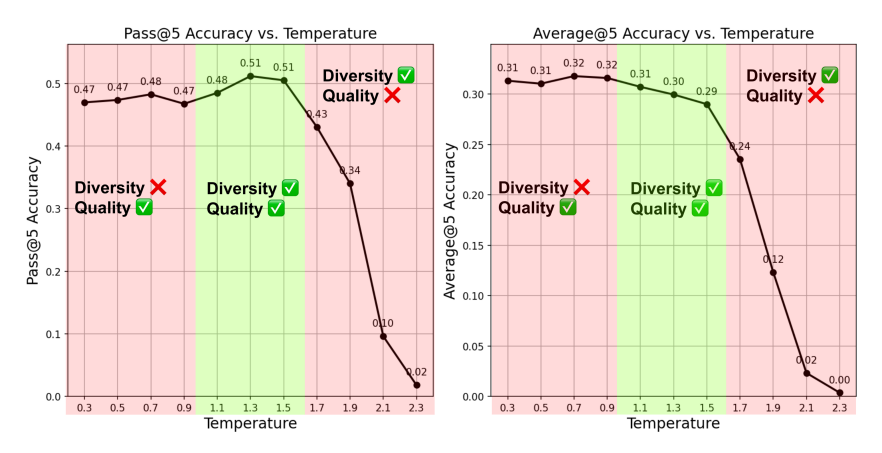


Figure 8: Performance analysis across different sampling temperatures on MATH500. The plot shows Pass@5 and Average@5 scores, revealing three distinct regions: low temperatures with high accuracy but low diversity, high temperatures with preserved diversity but degraded accuracy, and the middle region offering the desired trade-off. We select T=1.2 for our RL training.

633 G Inpainting Generation Qualitative Examples

Blue text: Question Prompt Green text: Injected Hints Black text: Inpainted Generation

Problem: Circle C has radius 6 cm. How many square centimeters are in the area of the largest possible inscribed triangle having one side as a diameter of circle C?

Inpainting Input At Denosing Step 0:

```
<|start_header_id|>user<|end_header_id|>
Respond in the following format:
<reasoning>
</reasoning>
<answer>
\ boxed{<Your answer>}
</answer>
Circle $C$ has radius 6 cm. How many square centimeters are in the area
of the largest possible inscribed triangle having one side as a diameter of circle $C$?<|eot_id|><|start_header_id|>assistant<|end_header_id|>
Since the diameter is twice the radius, the base of the triangle will have
length $2 \setminus times 6 = 12$ cm.
To {<}|{\tt mdm\_mask}|{>}\dots{<}|{\tt mdm\_mask}|{>} , we want the height to be as large
of the triangle is the distance from the midpoint of the base to the
circumference of the circle.
This is equal to the radius of the circle, <\!|\!\,\text{mdm\_mask}\,|\!>\ldots<\!|\!\,\text{mdm\_mask}\,|\!>
<|mdm_mask|>...<|mdm_mask|> <|mdm_mask|>...<|mdm_mask|>
12 \ times <|mdm_mask|>...<|mdm_mask|>
```

Inpainted Generation After Denoising:

```
We know to find the largest possible inscribed triangle in circle $C$, the base
of the triangle should be the diameter of the circle.
Since the diameter is twice the radius, the base of the triangle will have
length $2 \setminus times 6 = 12$ cm.
To find the largest possible area of the triangle, we want the height to be
as large as possible.
The largest possible height of the triangle is the distance from the midpoint of
the base to the
circumference of the circle.
This is equal to the radius of the circle, which is 6 cm.
Therefore, the area of the largest possible inscribed triangle is given by the
formula for the area of a triangle, which is \$\ frac{1}{2} \setminus times \setminus textbase
\ times \ textheight = \ frac{1}{2} \ times 12 \ times 6 = 36$$ square centimeters.
</reasoning>
<answer>
\ boxed{36}
</answer>
```

634 H Evaluation Hyperparameters

We evaluate all models with a fixed decoding setup per benchmark. Unless otherwise noted, the same prompts and decoding hyperparameters are applied to both LLaDA-8B-Instruct and LLaDA-1.5.

Table 3: Evaluation hyperparameters by benchmark.

Benchmark	Temp.	Block Len.	Diffusion Steps	Gen. Len.	Metric
GSM8K	0.0	32	512	512	pass@1
MATH500	0.0	32	512	512	pass@1
AMC	0.5	128	512	512	avg@16
Minerva	0.0	128	512	512	pass@1

I Prompt for SFT traces revision

Prompt for SFT traces revision sent to LLaMA 4 Maverick

Please rewrite the original solution to make it more concise and easier to understand without changing the details. Please put the explanation in the solution between <reasoning> and </reasoning> and put the final numerical answer between <answer> and </answer> in boxed format. Please shorten or rewrite the rewritten solution to a random length between 100 and 1000 words while keeping sufficient details of the reasoning steps. Please do not return anything other than the rewritten solution.

Example:

<reasoning>

XXX

</reasoning>

<answer>

 $\boxed{14}$

</answer>

Original solution: {generations}.

Your response:

SFT trace before rewritten by LLaMA 4 Maverick Problem: Find all primes between 1 and 15.

<think>

Okay, so I need to find all the prime numbers between 1 and 15. Hmm, let's start by remembering what a prime number is. From what I recall, a prime number is a natural number greater than 1 that has no positive divisors other than 1 and itself. So, numbers like 2, 3, 5, etc., are primes because you can't divide them evenly by any other number besides 1 and the number itself. On the other hand, numbers like 4, 6, 8, and so on are not primes because they can be divided by other numbers. For example, 4 can be divided by 2, so it's not prime. Alright, so the task is to list all primes between 1 and 15. Let me list out all numbers from 1 to 15 first to check them one by one. The numbers are: 1, 2, 3, 4, 5, 6, 7, 8, 9, 10, 11, 12, 13, 14, 15.

Now, let's go through each number and see if it's prime. Starting with 1. Wait, I remember that by definition, prime numbers are greater than 1. So 1 is not considered a prime. So we can skip 1.

Next up is 2. Let's check if 2 is prime. The divisors of 2 are 1 and 2. There are no other divisors, so yes, 2 is a prime number.

Moving on to 3. Similarly, the divisors are 1 and 3. No other numbers divide into 3, so 3 is prime.

Next is 4. Let's check divisors. 4 divided by 2 is 2, which is an integer, so 4 is not prime. It can be divided by 2, so it's composite.

Then 5. The divisors of 5 are 1 and 5. No other numbers divide into 5, so 5 is prime.

- 6. Checking divisors. 6 divided by 2 is 3, so it's divisible by 2 and 3. Not prime.
- 7. Divisors are 1 and 7. No other divisors, so 7 is prime.
- 8. Divided by 2 gives 4, so 8 is not prime.
- 9. Divided by 3 gives 3, so 9 is not prime (since 3 times 3 is 9).
- 10. Divided by 2 is 5, so 10 is not prime.
- 11. Let's see, 11. Divided by 2? 11 divided by 2 is 5.5, not an integer. Divided by 3? 11 divided by 3 is approximately 3.666... Not an integer. Divided by 4? 2.75, nope. 5? 2.2, nope. Since 11 is a prime number because none of these divisions result in integers, so 11 is prime. 12. Divided by 2 is 6, so composite.
- 13. Checking divisors. 13 divided by 2 is 6.5, 13 divided by 3 is about 4.333..., 4? 3.25, 5? 2.6, 6? 2.166... None of these are integers. So 13 is prime.
- 14. Divided by 2 is 7, so composite.
- 15. Divided by 3 is 5, so composite.

Let me recap the numbers between 1 and 15 and their primality:

- 1: Not prime
- 2: Prime
- 3: Prime
- 4: Not
- 5: Prime
- 6: Not
- 7: Prime
- 8: Not
- 9: Not
- 10: Not
- 11: Prime
- 12: Not
- 13: Prime
- 14: Not
- 15: Not

So compiling the primes from this list: 2, 3, 5, 7, 11, 13.

Wait a second, let me verify each one again just to be sure I didn't make a mistake.

Starting with 2: Definitely prime. It's the only even prime.

- 3: Prime, yes.
- 5: Prime, yes.
- 7: Prime. Correct.

11: Let's check again. 11 divided by 2 is not whole. 3? 3*3 is 9, 3*4 is 12. So no. 5? 5*2 is 10, 5*3 is 15. So 11 is prime.

13: Similarly, 13 divided by 2 is 6.5, 3 is 4.333, 5 is 2.6. So, prime.

Yes, those all check out. So primes between 1 and 15 are 2, 3, 5, 7, 11, and 13.

But hold on, sometimes people might make a mistake with 9. Wait, 9 is 3 times 3, so that's composite, which I had down. 15 is 3 times 5, composite. So all the non-primes are accounted for.

Is there any number I might have missed? Let's see. Let's list all numbers again:

2, 3, 5, 7, 11, 13. Are there any others?

Well, 1 is excluded. 4,6,8,9,10,12,14,15 are composite. So no, those six numbers are all primes between 1 and 15.

Wait, but the question says "between 1 and 15." Does that include 15? Hmm, the wording is "between 1 and 15," which could be a bit ambiguous. But usually, when someone says "between 1 and 15," they mean including both endpoints. However, since 15 is composite, it's excluded either way. So primes are 2,3,5,7,11,13.

Yes, that seems correct. I don't think I made any mistakes here. Let me cross-verify with another method, like the Sieve of Eratosthenes. The Sieve is a method where you list all numbers and cross out multiples.

Starting with 2, cross out multiples: 4,6,8,10,12,14.

Then 3, cross out multiples: 6,9,12,15.

Then 5, cross out 10,15.

7, cross out 14.

11 and 13 are primes, and their multiples are beyond 15. So remaining numbers are 2,3,5,7,11,13. Which matches our previous list.

Therefore, the primes between 1 and 15 are 2,3,5,7,11,13.

Final Answer

The primes between 1 and 15 are $\boxed{2}$, $\boxed{3}$, $\boxed{5}$, $\boxed{7}$, $\boxed{11}$, and $\boxed{13}$. </think>

To find all the prime numbers between 1 and 15, we start by recalling that a prime number is a natural number greater than 1 that has no positive divisors other than 1 and itself. We then check each number from 1 to 15:

- **1**: Not a prime number (by definition).
- **2**: Prime (divisors: 1, 2).
- **3**: Prime (divisors: 1, 3).
- **4**: Not prime (divisible by 2).
- **5**: Prime (divisors: 1, 5).
- **6**: Not prime (divisible by 2, 3).
- **7**: Prime (divisors: 1, 7).
- **8**: Not prime (divisible by 2).
- **9**: Not prime (divisible by 3).
- **10**: Not prime (divisible by 2, 5).
- **11**: Prime (divisors: 1, 11).
- **12**: Not prime (divisible by 2, 3, 4, 6).
- **13**: Prime (divisors: 1, 13).
- **14**: Not prime (divisible by 2, 7).
- **15**: Not prime (divisible by 3, 5).

Using the Sieve of Eratosthenes method to cross out non-prime numbers confirms the primes listed above. Therefore, the prime numbers between 1 and 15 are:

2, 3, 5, 7, 11, 13

SFT trace after rewritten by LLaMA 4 Maverick **Problem:** Find all primes between 1 and 15.

</answer>

```
<reasoning>
To find all the prime numbers between 1 and 15, we recall that a prime number is a natural
number greater than 1 that has no positive divisors other than 1 and itself.
We then check each number from 1 to 15 to determine if it is prime.
- **1**: Not a prime number (by definition).
- **2**: Prime (divisors: 1, 2).
- **3**: Prime (divisors: 1, 3).
- **4**: Not prime (divisible by 2).
- **5**: Prime (divisors: 1, 5).
- **6**: Not prime (divisible by 2, 3).
- **7**: Prime (divisors: 1, 7).
- **8**: Not prime (divisible by 2).
- **9**: Not prime (divisible by 3).
- **10**: Not prime (divisible by 2, 5).
- **11**: Prime (divisors: 1, 11).
- **12**: Not prime (divisible by 2, 3, 4, 6).
- **13**: Prime (divisors: 1, 13).
- **14**: Not prime (divisible by 2, 7).
- **15**: Not prime (divisible by 3, 5).
The Sieve of Eratosthenes method confirms the primes listed above.
</reasoning>
<answer>
 2, 3, 5, 7, 11, 13
```